Spin-Lattice Relaxation Times of Cu^{2+} in $CuSO_4 \cdot 5H_2O$ and Yb^{3+} in CaF_2 by Nuclear Dynamic Polarization

J. S. KARRA AND HARVEY WALDMAN*
Department of Physics, Temple University, Philadelphia, Pennsylvania 19122
(Received 6 January 1969)

Dynamic polarization of protons in $CuSO_4 \cdot 5H_2O$-doped $ZnSO_4 \cdot 7H_2O$ and F^{19} nuclei in Yb^{3+}-doped calcium fluoride (trigonal sites) has been observed in the range 1.6–4.2°K. Concentration, temperature, and microwave-power dependencies of the polarization and relaxation times of the nuclei are measured, and these dependencies are deduced for the Cu^{2+} and Yb^{3+} electron relaxation times. Copper electrons are found to relax mainly by the direct process, but the Orbach process is observed for ytterbium electrons above the range 3.6–4.2°K. Below this range, the direct process predominates. All samples indicate spin-diffusion-limited processes. A general expression is derived for the Orbach process of a Kramer's salt; it is applied to Cu^{2+} and Yb^{3+} and compared with the values deduced from the measurements. The wave functions of the ground states of Yb^{3+} in a trigonal site are calculated from ESR measurements and used in the above analysis. The first excited orbital-level splitting of ytterbium is calculated from the temperature at which the Orbach process relaxation rate becomes greater than that of the direct process. A lower bound for this splitting is obtained for copper.

I. INTRODUCTION

NUCLEAR dynamic polarization[1–6] provides a direct means of studying nuclear spin-lattice relaxation, and, in samples containing small numbers of paramagnetic ions, the nuclei may preferably relax to the lattice through the electron spins, thereby giving information on the electron-spin-lattice relaxation mechanisms. Nuclear relaxation does not necessarily proceed from the nuclei directly to the electrons but may be accomplished by transport of energy over large distances by nuclear spin diffusion. In this way energy is transferred from nucleus to nucleus until it reaches one which can relax through the paramagnetic ions. Dynamic polarization offers positive information on whether the nuclei experience spin diffusion or only relax to the lattice through the direct interaction with the electrons.

Once the presence or absence of spin diffusion is confirmed, the mechanism by which electrons relax to the lattice may be deduced. Various electron spin-lattice relaxation processes may be identified by their temperature dependencies. These may be obtained from the temperature dependence of the nuclear relaxation.

If the concentration of paramagnetic impurities is large, the electrons may experience a phonon bottleneck as discussed in an earlier paper[6] by one of the authors (JSK). The effect of a phonon bottleneck may be circumvented by dynamic polarization. Therefore, not only are the nuclear spin-lattice relaxation rates and their temperature dependencies measured, but the electron spin-lattice relaxation rates and their relaxation processes may be deduced whether or not a phonon bottleneck is present.

Dynamic polarization of nuclei is superior in many respects to the progressive saturation method and to some extent to pulse techniques. In the case of wide and inhomogeneous ESR lines saturation is difficult; and the relaxation rate measured is some average of the rates of the various spin packets of the line. In addition, the pulse technique requires large amounts of rf power. In the case of extremely dilute concentrations (10^{-3}%), the main contribution to the width of a homogeneous line is due to spin-lattice relaxation. In the samples studied here, however, the linewidth is too large to be explained by this. This could be due to inhomogeneous broadening caused by interaction with the F^{19} nuclei and hyperfine interaction with Yb^{173} nuclei. In such cases it is difficult to separate spin-lattice relaxation from the observed linewidth. Therefore, the ESR linewidth cannot be used to study spin-lattice relaxation and its temperature dependence.

In this paper the electron spin-lattice rates of two systems are studied, one an iron-group ion, and the other a rare-earth ion. Both systems are measured at temperatures in the range 1.6–4.2°K. The main difference between these two classifications, for our purposes, is the size of spin-orbit coupling relative to the magnitude of the crystal field. In the iron group it is smaller and in the rare-earth group it is larger.

The iron-group ion, Cu^{2+} in $CuSO_4 \cdot 5H_2O$, is diluted $\frac{1}{4}$–6% in $ZnSO_4 \cdot 7H_2O$. Pure copper sulphate, one of the few compounds of the $5H_2O$ structure, was studied at room temperature for g-tensor values, crystal field parameters, and hyperfine structure constants.[7,8] No investigation was conducted at liquid-helium temperatures, however, and no investigation of dilute samples

* Paper based upon a dissertation by Harvey Waldman submitted in partial fulfillment of the requirements for the Ph.D. degree at Temple University.

[1] A. Abragam and W. G. Proctor, Compt. Rend. **246**, 2253 (1958).

[2] M. Abraham, M. A. H. McCausland, and F. N. H. Robinson, Phys. Rev. Letters **2**, 449 (1959).

[3] N. Borghini and A. Abragam, Compt. Rend. **248**, 1803 (1959).

[4] G. E. Schacher, Phys. Rev. **135**, A185 (1964).

[5] C. D. Jeffries and O. S. Leifson, Phys. Rev. **122**, 1781 (1961).

[6] J. S. Karra, R. Clarkson, and T. Sato, Phys. Rev. **175**, 479 (1968).

[7] D. M. S. Bagguley and J. H. E. Griffiths, Proc. Roy. Soc. (London) **201**, 366 (1952).

[8] M. H. L. Pryce, Nature **162**, 539 (1948).

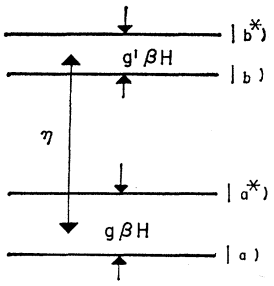

FIG. 1. Energy-level diagram of a general Kramer's salt in the presence of a magnetic field.

was performed at all. Relaxation data are almost nonexistent. At low temperatures the presence of exchange interactions of the concentrated sample make it ferromagnetic. Therefore, no studies of their relaxation times may be made. Also, all existing relaxation theories are applicable to dilute paramagnetic samples only. Dilution will reduce the exchange interaction and make low-temperature experiments possible, but dilute single crystals are very difficult to grow. To circumvent this problem the samples studied here are prepared in polycrystalline form.

Because of the asymmetry of the g tensor and the presence of unresolved hyperfine structure, the copper ESR line is wide and inhomogeneous in polycrystalline samples. This makes the method of dynamic polarization particularly suited to study these samples. The electron-nuclear interaction utilized is between the copper $3d^9$ electrons and the protons of the water of hydration.

The rare-earth ion is Yb^{3+} doped 0.01–0.1% into trigonal sites of CaF_2, forming a Kramer's ion. Dynamic polarization is between the Yb^{3+} ($4f^{13}$) electrons and the F^{19} nuclei. ESR measurements of Yb^{3+} in these sites have been made by Low and Rosenberger,[9] and Low and Ranon.[10] Low and Rosenberger calculated the ground-state wave function. Relaxation measurements were also made by Bierig, Weber, and Warshaw[11] but only for the cubic and tetragonal sites.

In Sec. II an order of magnitude calculation of the spin-lattice relaxation rate in a Kramer's salt will be made for the Orbach process. It will then be applied to Cu^{2+} and Yb^{3+}.

The experimental procedure will be briefly outlined in Sec. III, nuclear relaxation will be discussed in Sec. IV and the results will be presented in Sec. V.

II. SPIN-LATTICE RELAXATION

A. Electron

An electron in an excited state may relax to its ground state by transferring its excitation energy to the phonon system of the lattice. The characteristic rate of this transfer $1/T_1$ depends on the spin-phonon interaction Hamiltonian and the ability of the phonon system to absorb this energy. From time-dependent perturbation theory,[6]

$$1/T_1=2W_{if}=(4\pi/h)|(f|H_{sp}|i)|^2\rho(h\nu), \quad (1)$$

where $\rho(h\nu)$ is the phonon density at energy $h\nu$ and therefore a measure of the ability of the lattice to absorb a quantum of this energy and $(f|H_{sp}|i)$ is the matrix element of the spin-phonon interaction Hamiltonian between the initial and final states of the spin-lattice system. As in Ref. 6, only an order of magnitude attempt will be made to calculate $(f|H_{sp}|i)$ by expressing the amplitudes of the variations of the local crystal field in terms of the amplitudes of the lattice vibrations. Equation (1) will be evaluated for the Orbach process[12–15] of a general Kramer's salt, and compared with the direct process. It will then be shown that a salt primarily relaxing by the direct process at low temperatures will relax primarily by the Orbach process once a characteristic temperature T^* is exceeded. Experimental evidence of this will be presented.

The phonon distribution may be written[6]

$$\rho(h\nu)=[4\pi(h\nu)^2V/h^3v^3](e^{h\nu/kT}-1)^{-1}, \quad (2)$$

where V is the volume of the crystal; v is the velocity of sound in the lattice; and T is the lattice temperature. This equations holds up to $\nu_{max}=k\Theta_D/h\simeq10^{13}$ Hz, where Θ_D is the Debye temperature.

1. Orbach Process

The Orbach process may be defined as a transition between two orbital levels of opposite spin which results in a change of Zeeman populations. If η is the energy difference between the ground orbital and the next highest orbital then the energy of the relaxing phonon is $h\nu=\eta$ (see Fig. 1). Therefore,

$$\rho_0(h\nu)=4\pi\eta^2V/h^3v^3(e^{\eta/kT}-1)^{-1}; \quad (3)$$

for $kT\ll\eta$,

$$\rho_0=4\pi\eta^2V\exp(-\eta/kT)/h^3v^3, \quad (4)$$

and for $kT\gg\eta$,

$$\rho_0=4\pi\eta VkT/h^3v^3. \quad (5)$$

2. Direct Process

From Ref. 6,

$$\rho_D=4\pi(g\beta H)^2VkT/h^3v^3. \quad (6)$$

H_{sp} may be expressed as a linear sum of terms transforming as the spherical harmonics

$$H_{sp}=\sum_{n,m}A_n{}^m\epsilon_n{}^m\hat{V}_n{}^m, \quad (7)$$

where $\epsilon_n{}^m$ is that portion of the strain transforming as the spherical harmonic $Y_n{}^m$, $\hat{V}_n{}^m$ is that portion of the crystal field potential transforming as $Y_n{}^m$, and $A_n{}^m$

[9] W. Low and U. Rosenberger, Compt. Rend. **254**, 1771 (1962).
[10] W. Low and U. Ranon, *Paramagnetic Resonance*, edited by W. Low (Academic Press Inc., New York, 1963), Vol. 1.
[11] R. W. Bierig, M. J. Weber, and S. I. Warshaw, Phys. Rev. **134**, A1504 (1964).
[12] J. Waller, Z. Physik **79**, 370 (1932).
[13] R. DeL. Kronig, Physica **6**, 33 (1939).
[14] C. B. P. Finn, R. Orbach and W. P. Wolf, Proc. Phys. Soc. (London) **77**, 261 (1961).
[15] R. Orbach, Proc. Roy. Soc. (London) **A264**, 458 (1961).

is a coefficient. As in Ref. 15, only an average strain will be considered, $\epsilon=\partial R/R$, where ∂R is the displacement of a ligand from its equilibrium position R. This displacement by an acoustic wave may be expressed as a function of the amplitude of that wave q:

$$\partial R=2\pi Rq/\lambda=2\pi R/\lambda(h/2M\nu)^{1/2} \quad (8)$$

or

$$\epsilon=\partial R/R=1/v(2h\nu/M)^{1/2}. \quad (9)$$

This differs from Eq. (5) of Ref. 6 by a factor Δ, the average crystal field splitting. In that reference Δ was factored from the matrix element of the crystal-field perturbation at the ionic site and introduced into the expression for the amplitude of the lattice displacement. In this paper it is retained in the matrix element.

Combining Eqs. (7) and (9),

$$|(f|H_{\rm sp}|i)|^2=\frac{2h\nu}{v^2M}|(f'|\sum_{nm}A_n{}^mV_n{}^m|i')|^2, \quad (10)$$

where i' and f' refer to the initial and final orbital electron states. For the Orbach process,

$$(1/T_1)_0=\frac{(4\pi)^3\eta^3}{h^4v^5\rho}e^{-\eta/kT}|(a|\sum_{nm}A_n{}^mV_n{}^m|b^*)\times(b|\sum_{nm}A_n{}^mV_n{}^m|a^*)|, \quad (11)$$

and for the direct process,

$$(1/T_1)_D=\frac{(4\pi)^3(g\beta H)^4kT}{h^4v^5\rho}|(a|\sum_{nm}A_n{}^mV_n{}^m|a^*)|^2, \quad (12)$$

where ρ is the mass density.

B. Yb in Trigonal State

Free Yb^{3+} ($4f^{13}$) may be treated as a hole in the $4f$ shell. The only allowable state ^2F is split by spin-orbit coupling into two states, $^2F_{5/2}$ and $^2F_{7/2}$. According to Hund's rules the $J=\frac{7}{2}$ state is lowest, and this has been observed by ESR and the splitting has been measured to be 9000 to 10 000 cm^{-1}.[16]

When placed in a field of cubic symmetry, the $^2F_{7/2}$ level splits into Γ_7 and Γ_6 doublets and a Γ_8 quartet. The Γ_7 state has been observed to be lowest.[17] If the cube is stretched along a body diagonal [111], the quartet is split and the $^2F_{7/2}$ state is now composed of four Kramer's degenerate doublets which will be labeled Γ_6', Γ_7', $\Gamma_{8\alpha}'$, and $\Gamma_{8\beta}'$.

ESR of Yb^{3+} in trigonal sites of CaF_2 was observed by Low and Rosenberger,[9] and Low and Ranon.[10] They confirmed that the symmetry axis was along a body diagonal and measured the g and hyperfine A tensors. From the g values they calculated the ground state

$$\Phi=0.941|\pm\tfrac{1}{2})+0.264|\pm\tfrac{7}{2})+0.208|\mp\tfrac{5}{2}), \quad (13)$$

where the lower set of signs corresponds to the Kramer's conjugate of the state represented by the upper set of signs.

In analyzing the ground state of Yb^{3+} it would be convenient to have the $^2F_{7/2}$ wave function quantized along the [111] direction. This was accomplished by Sroubek *et al.*[18]

In this analysis of the ground state of Yb it will be assumed that the effect of the trigonal field is smaller than that of the cubic field and therefore, to the first order, the trigonal wave functions equal the cubic wave functions,[18] $\Gamma_6'\simeq\Gamma_6$, $\Gamma_7'\simeq\Gamma_7$, $\Gamma_{8\alpha}'\simeq\Gamma_{8\alpha}$, $\Gamma_{8\beta}'\simeq\Gamma_{8\beta}$. The functions $|\pm\frac{3}{2})$ are not mixed by the trigonal field and therefore $\Gamma_{8\beta}'=\Gamma_{8\beta}$ exactly.

By considering the Hamiltonian of a cubic plus trigonal field quantized along the trigonal field axis[18,19] and operating on the cubic wave functions, the trigonal field wave functions may be obtained. They are

$$\begin{aligned}
|\Gamma_6')&=\pm0.328|\pm\tfrac{1}{2})-0.737|\mp\tfrac{5}{2})+0.591|\pm\tfrac{7}{2})\\
&=-0.298|\Gamma_7)+0.940|\Gamma_6)+0.166|\Gamma_8),\\
|\Gamma_{8\alpha}')&=\pm0.0714|\pm\tfrac{1}{2})+0.643|\mp\tfrac{5}{2})+0.762|\pm\tfrac{7}{2})\\
&=-0.270|\Gamma_7)-0.250|\Gamma_6)+0.929|\Gamma_8),\\
|\Gamma_{8\beta}')&=|\pm\tfrac{3}{2})\\
&=|\Gamma_{8\beta}),\\
|\Gamma_7')&=\pm0.942|\pm\tfrac{1}{2})+0.208|\mp\tfrac{5}{2})-0.264|\pm\tfrac{7}{2})\\
&=0.916|\Gamma_7)+0.232|\Gamma_6)+0.328|\Gamma_8).
\end{aligned} \quad (14)$$

These transformations are used to evaluate the matrix elements of J_x in Eq. (17).

Using the splitting $E_{8\alpha}'$-E_7' as the scale factor δ, and to order of magnitude

$$(\Gamma_{8\alpha}'^*|\sum_{nm}A_n{}^mV_n{}^m|\Gamma_7')\simeq\delta. \quad (15)$$

Since $\eta=\delta$, from Eq. (11)

$$(1/T_1)_0=[(4\pi)^3\delta^5/h^4v^5\rho]e^{-\delta/kT}. \quad (16)$$

Also, if the magnetic field is perpendicular to the quantization axis,

$$\begin{aligned}
&(\Gamma_7'^*|\sum_{nm}A_n{}^mV_n{}^m|\Gamma_7')\\
&=g_\perp\beta H\sum_p 1/(E_p'-E_7')(\Gamma_7'|J_x|\Gamma_p'^*)\times(\Gamma_p'^*|\sum_{nm}A_n{}^mV_n{}^m|\Gamma_7'^*)\\
&\simeq(g_\perp\beta H/\delta)(\Gamma_7'|J_x|\Gamma_{8\alpha}'^*)\times(\Gamma_{8\alpha}'^*|\sum_{nm}A_n{}^mV_n{}^m||\Gamma_7'^*)\\
&\simeq-0.150g_\perp\beta H,
\end{aligned} \quad (17)$$

and

$$(1/T_1)_D=0.0225(4\pi)^3(g_\perp\beta H)^4kT/h^4v^5\rho. \quad (18)$$

[16] G. H. Dieke and H. M. Crosswhite, Appl. Opt. **2**, 675 (1963).
[17] M. Abraham, R. A. Weeks, G. W. Clark, and C. B. Finch, Phys. Rev. **137**, A138 (1965).
[18] Z. Sroubek, M. Tachiki, P. H. Zimmerman, and R. Orbach, Phys. Rev. **165**, 435 (1968).
[19] S. A. Al'tshuler and B. M. Kozyrev, *Electron Paramagnetic Resonance* (Academic Press Inc., New York, 1964).

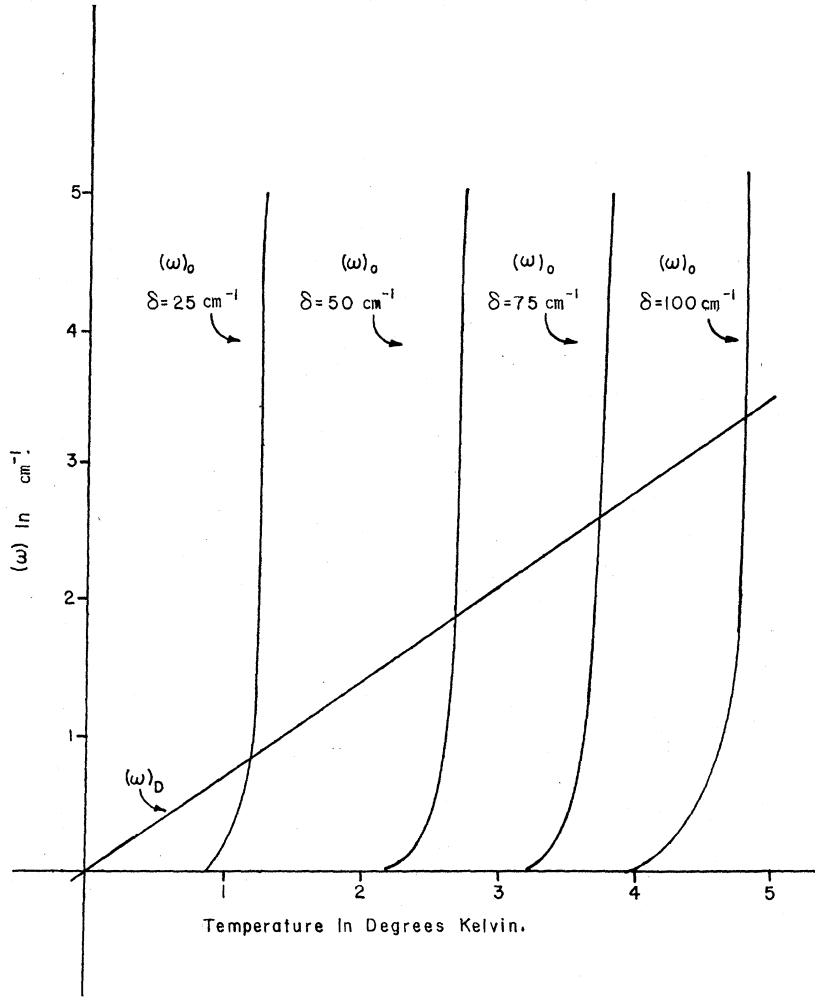

FIG. 2. Plot of functions $(w)_0$ and $(w)_D$ for Yb^{3+} in CaF_2.

If a function is constructed,

$$(w)=(1/T_1)[h^4v^5\rho/0.0225(4\pi)^3(g_1\beta H)^4]. \quad (19)$$

This function will be for the Orbach process,

$$(w)_0=[44.4\delta^5/(g_1\beta H)^4]e^{-\delta/kT}, \quad (20)$$

and for the direct process,

$$(w)_D=kT. \quad (21)$$

Using $g_1\beta H=\frac{1}{3}$ cm^{-1}, $(w)_0$ and $(w)_D$ are plotted in Fig. 2. Since the total relaxation rate is $(1/T_1)_0+(1/T_1)_D$, for a given value of δ, the relaxation process (as can be seen in Fig. 2) will go from a predominantly direct process to an Orbach process at a temperature T^*. Conversely, if T^* is known, δ may be determined. As will be shown later T^* was observed to occur in the region 3.6–4.2°K, resulting in a splitting $\delta\simeq 80$ cm^{-1}.

The matrix element $(\Gamma_{8\alpha}{}'^*|\sum_{nm}A_n{}^mV_n{}^m|\Gamma_7')$ was evaluated to order of magnitude; therefore, Eqs. (16) and (18) are only to this accuracy. However, the form of these two equations and the ratio of their coefficients $[C]$ are known more exactly. If T^* is defined as the temperature at which $(1/T_1)_0=(1/T_1)_D$, then

$$(w)_D=(w)_0=kT^*=C\delta^5e^{-\delta/kT^*}, \quad (22)$$

and for $\delta=80$ cm^{-1}, $T^*=4.0$°K,

$$\partial\delta/\delta=0.04\partial C/C. \quad (23)$$

Or, δ may be evaluated to at least an order of magnitude more accurately than C and principally depends on the form of Eqs. (16) and (18). Therefore, the splitting δ may be determined to the accuracy of the measurement of T^*, say, ± 10 cm^{-1}.

The over-all cubic field splitting is 65 cm^{-1}. Previous reports[20,21] for this splitting have ranged from 16 to 800 cm^{-1}.

The linewidth of extremely dilute samples should be a measure of spin-lattice relaxation rate provided the lines are not inhomogeneously broadened. Inhomogeneous broadening may be due to an anisotropic g tensor (absent in single crystals), unresolved hyperfine structure, a small degree of covalency, dipolar broad-

[20] W. Hayes and J. W. Twidell, J. Chem. Phys. **35**, 1521 (1961).
[21] M. J. Weber and R. W. Bierig, Phys. Rev. **134**, A1491 (1964).

ening due to dissimilar spins, or even the inhomogeneity in the external magnetic field. The Yb^{3+} ESR linewidth is about 20 G, which corresponds to a rate of $\simeq 3\times 10^8$ sec^{-1}. The electron spin-lattice relaxation rate $1/T_{1e}$ as will be shown, may be as great as 1000 sec^{-1} at 4.2°K, clearly contributing very little to the linewidth.

C. Cu^{2+} in Tetragonal Site

Cu^{2+} $(3d^9)$, when placed in a strong cubic field, is split into a nonmagnetic orbital ground doublet, $(x^2-y^2)(3z^2-r^2)$, and a triplet, $(xy)(xz)(yz)$.[6] The tetragonal field will split the doublet into two orbital singlets, and spin-orbit coupling and the Zeeman operator may be treated as perturbations which mix the wave functions. The wave functions are evaluated in Ref. 6, Eqs. (8)–(11), and (14), and are reproduced here only to first-order mixing in λ/Δ and $g\beta H/\Delta$, since Van Vleck cancellations do not occur:

$$\begin{aligned}
\Psi_\alpha^{(1)} &= |x^2-y^2,\alpha\rangle + i\frac{(\lambda+g\beta H)}{\Delta}|xy,\alpha\rangle + \frac{i\lambda}{2\Delta}|yz,\alpha\rangle,\\
\Psi_\beta^{(1)} &= |x^2-y^2,\beta\rangle - i\frac{(\lambda-g\beta H)}{\Delta}|xy,\beta\rangle - \frac{i\lambda}{2\Delta}|yz,\alpha\rangle,\\
\Psi_\alpha^{(2)} &= |3z^2-r^2,\alpha\rangle + i\frac{\sqrt{3}\lambda}{2\Delta}|yz,\beta\rangle - \frac{\sqrt{3}\lambda}{2\Delta}|zx,\beta\rangle,\\
\Psi_\beta^{(2)} &= |3z^2-r^2,\beta\rangle - i\frac{\sqrt{3}\lambda}{2\Delta}|yz,\alpha\rangle + \frac{\sqrt{3}\lambda}{2\Delta}|zx,\alpha\rangle.
\end{aligned} \tag{24}$$

The energy-level diagram is shown in Fig. 3, with the state (x^2-y^2) arbitrarily shown lower than $(3z^2-r^2)$.

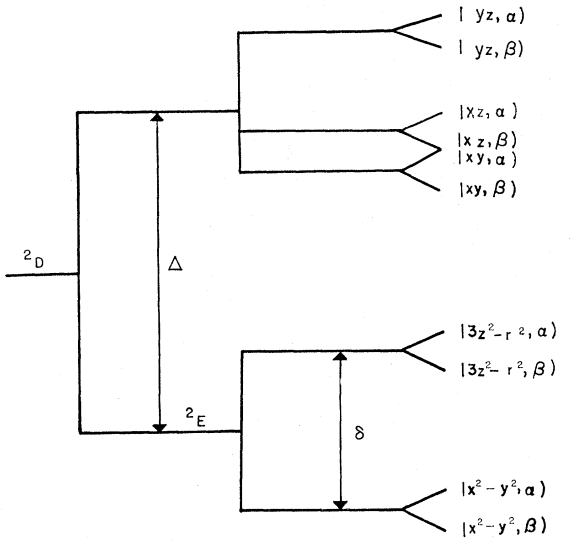

FIG. 3. Energy-level diagram of Cu^{2+} in tetragonal and magnetic fields.

1. Orbach Process

To lowest order in λ/Δ and $g\beta h/\Delta$, and using $\eta=\delta$,

$$\begin{aligned}
(\Psi_\beta^{(1)}|\sum_{nm} A_n{}^m V_n{}^m|\Psi_\alpha^{(2)}) &\simeq (\Psi_\alpha^{(1)}|\sum_{nm} A_n{}^m V_n{}^m|\Psi_\beta^{(2)})\\
&\simeq (\lambda/\Delta)(3z^2-r^2|\sum_{nm} A_n{}^m V_n{}^m|xy)\\
&\simeq \lambda
\end{aligned} \tag{25}$$

and

$$\begin{aligned}
\langle\Psi_\beta^{(2)}|\sum_{nm} A_n{}^m V_n{}^m|\Psi_\beta^{(1)}\rangle &= \langle 3z^2-r^2|\sum_{nm} A_n{}^m V_n{}^m|x^2-y^2\rangle,\\
\text{or}\quad (1/T_1)_0 &= [(4\pi)^3\delta^3\lambda^2/h^4v^5\rho]e^{-\delta/kT}.
\end{aligned} \tag{26}$$

Note the presence of λ^2 in this equation in the place of δ^2 in Eq. (16) for the rare-earth ion.

2. Direct Process

From Ref. 6

$$(1/T_1)_D = [2(4\pi)^3(g\beta H)^4/h^4v^5\rho](\lambda/\Delta)^2 kT. \tag{27}$$

As in Eqs. (20) and (21),

$$(w)_D = kT, \tag{28}$$

$$(w)_0 = [\Delta^2\delta^3/2(g\beta H)^4]e^{-\delta/kT}. \tag{29}$$

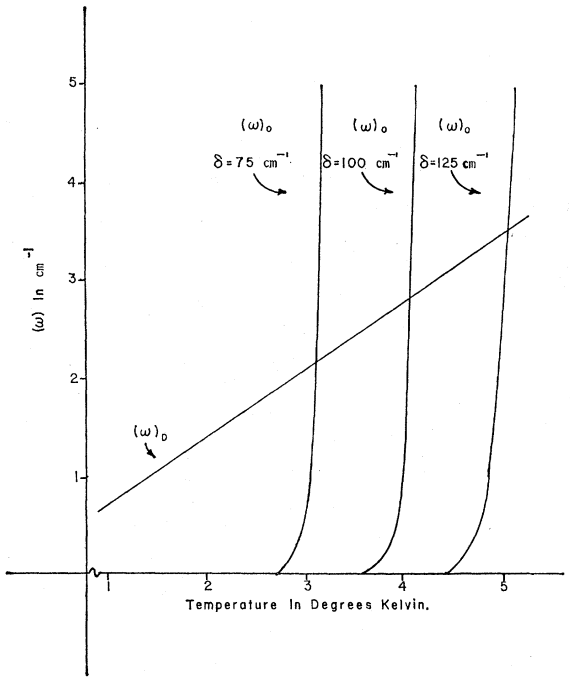

FIG. 4. Plot of functions $(w)_0$ and $(w)_D$ for Cu^{2+} in copper sulfate.

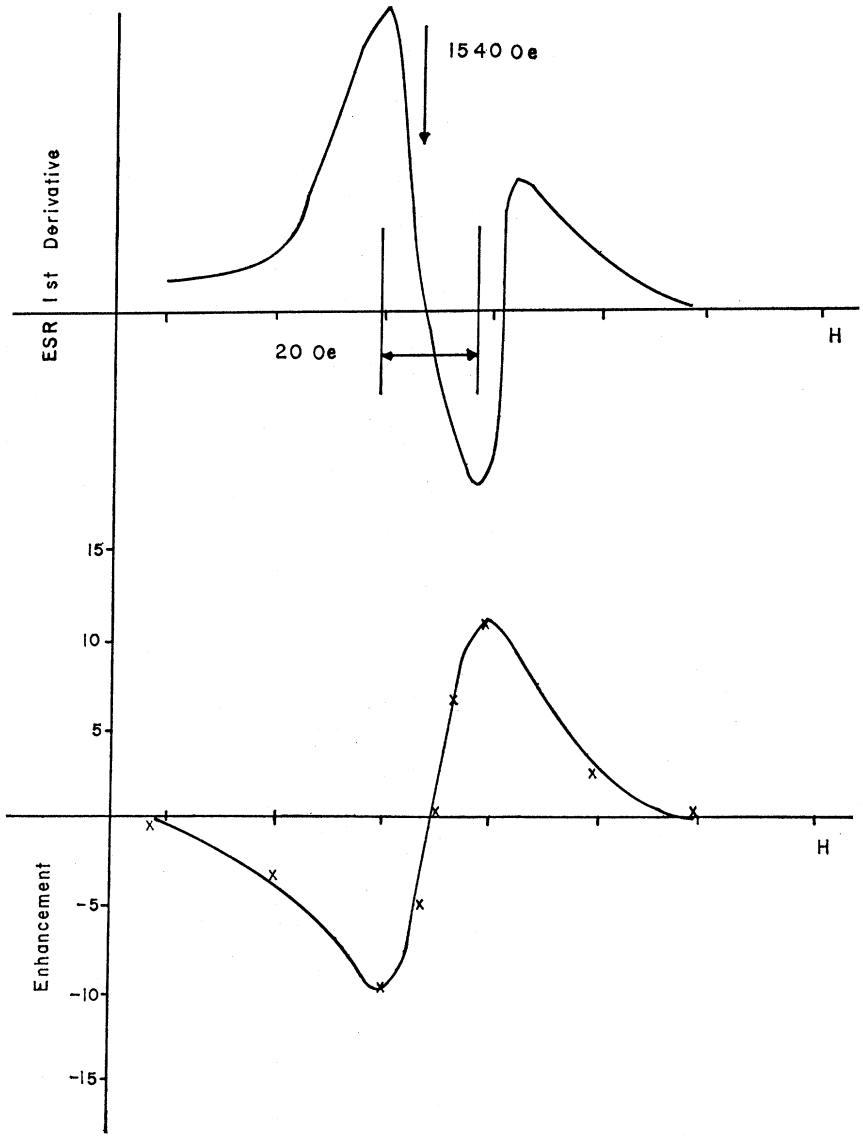

FIG. 5. ESR and enhancement versus magnetic field, 0.05% Yb^{3+} in CaF_2.

$(w)_0$ and $(w)_D$ are plotted in Fig. 4 using $\Delta = 12\,300$ cm^{-1} [22-24] and $g\beta H = \frac{1}{3}$ cm^{-1}.

Since the Orbach process was not detected up to the maximum experimental temperature of 4.2°K, Fig. 4 indicates that $\delta > 100$ cm^{-1}.

III. EXPERIMENTAL PROCEDURE

Dynamic polarization was observed by means of a double-resonance spectrometer consisting of a Varian V-4500 ESR spectrometer and a Modified Magnion G-502 NMR gaussmeter. The microwave frequency was 9.2 KMHz while proton resonance was observed at 13 MHz and fluorine resonance at 6 MHz.

Two Arra X110 diode microwave switches were used in series to permit dynamic double-resonance experiments.

All samples were immersed in liquid helium at 4.2°K and temperatures as low as 1.6°K were obtained by pumping on the helium bath.

Polycrystalline samples of dilute copper sulphate, with up to 10% Cu, were prepared by rapid cooling of a saturated solution of reagent grade $CuSO_4 \cdot 5H_2O$ and $ZnSO_4 \cdot 7H_2O$. The two reagents in proper proportions were dissolved in excess water, boiled to saturation, and cooled to room temperature. The sample was removed as a precipitate. The samples displayed a tendency to lose water of hydration and therefore were placed in sealed quartz tubes throughout these experiments.

The CaF_2 samples were purchased from Semi-Elements, Inc., Saxonburg, Pa.

[22] A. Abraham and M. H. L. Pryce, Proc. Roy. Soc. (London) **A206**, 164 (1951).
[23] H. Abe and K. Ono, J. Phys. Soc. Japan **11**, 947 (1956).
[24] J. Owen, Proc. Roy. Soc. (London) **A227**, 183 (1955).

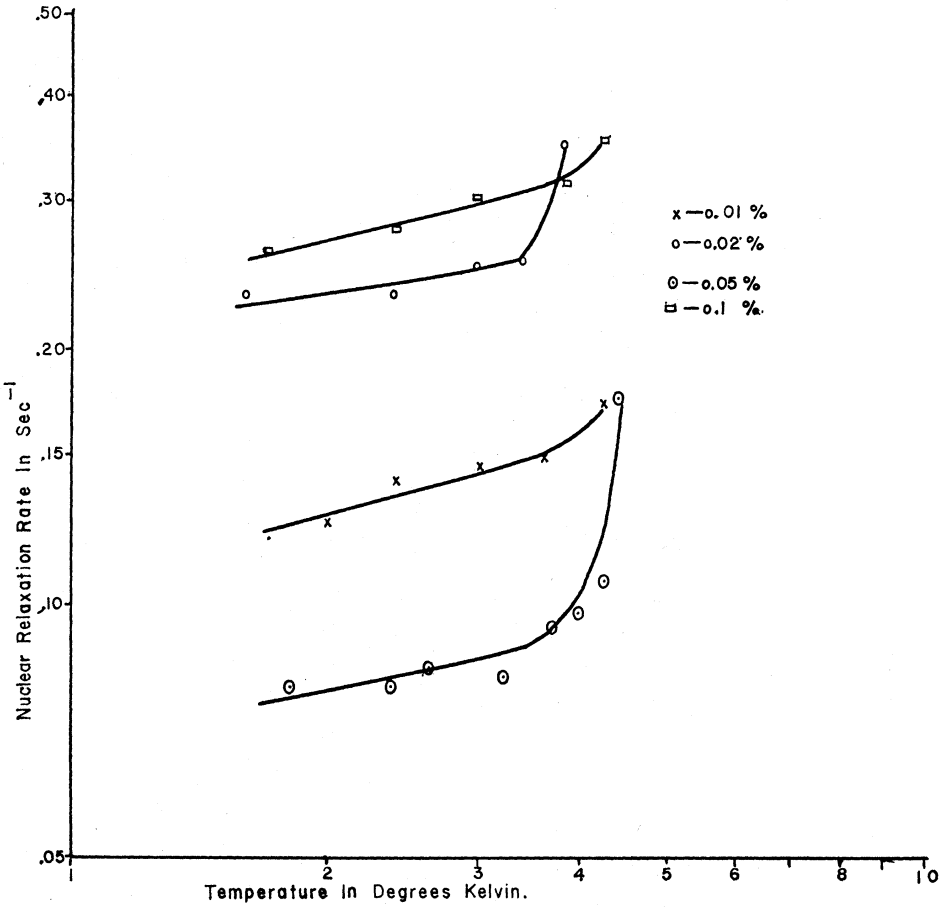

FIG. 6. Nuclear relaxation rate versus temperature, Yb^{3+} in CaF_2.

IV. NUCLEAR RELAXATION

Dynamic polarization may be used to study electron relaxation because the nuclei find that their best relaxation path is through the electrons of the paramagnetic site.

Spin-diffusion-limited process may be characterized by the following equation for nuclear polarization times[25]:

$$1/T_P = 8.5 N \Gamma^{1/4} D^{3/4}, \tag{30}$$

where N is the density of the paramagnetic ions, D is the nuclear spin-diffusion constant, and Γ is the microwave power. Measurement of $1/T_P$ versus microwave power, therefore, provides a means of determining if the polarization and relaxation processes are diffusion limited, since nondiffusion processes display a linear relationship between $1/T_P$ and Γ. Intermediate processes are possible and they display an exponent of Γ between $\frac{1}{4}$ and 1.

The nuclear relaxation rate has the following equation for spin-diffusion-limited processes[5]:

$$1/T_N = 8.5 N C^{1/4} D^{3/4}, \tag{31}$$

where

$$C = (2/5)\gamma_S^2 \gamma_I^2 \hbar^2 S(S+1) T_{1e}/(1+\omega_I^2 T_{1e}^2),$$
$$D = a^2/30\, T_{2n},$$

γ_S is the electron magnetogyromagnetic ratio, γ_I is the nuclear magnetogyromagnetic ratio, S is the electron spin, T_{1e} is the electron-lattice relaxation time, ω_I is the nuclear Larmor frequency, a is the internuclear distance, and T_{2n} is the nuclear spin-spin relaxation time. For $\omega_I^2 T_{1e}^2 \gg 1$, and for the spin-diffusion-limited process

$$1/T_{1e} \propto (1/T_N)^4. \tag{32}$$

As an example, the direct process, $1/T_{1e} \propto kT$, may be identified by experimentally demonstrating $1/T_N \propto (kT)^{1/4}$.

Nondiffusion-limited processes show $1/T_{1e} \propto 1/T_N$, but no simple relationship exists for intermediate processes.

V. RESULTS

Four CaF_2 samples containing 0.01%, 0.02%, 0.05%, and 0.1% Yb, respectively, were cleaved, oriented, and placed in the dynamic polarization apparatus. Little variation of the results was observed as a function of concentration. (See Table I.) Site symmetry and g-value measurements of Low and Rosenberger[9] were confirmed

[25] A. Abragam, *Principles of Nuclear Magnetism* (Oxford University Press, Cambridge, 1961).

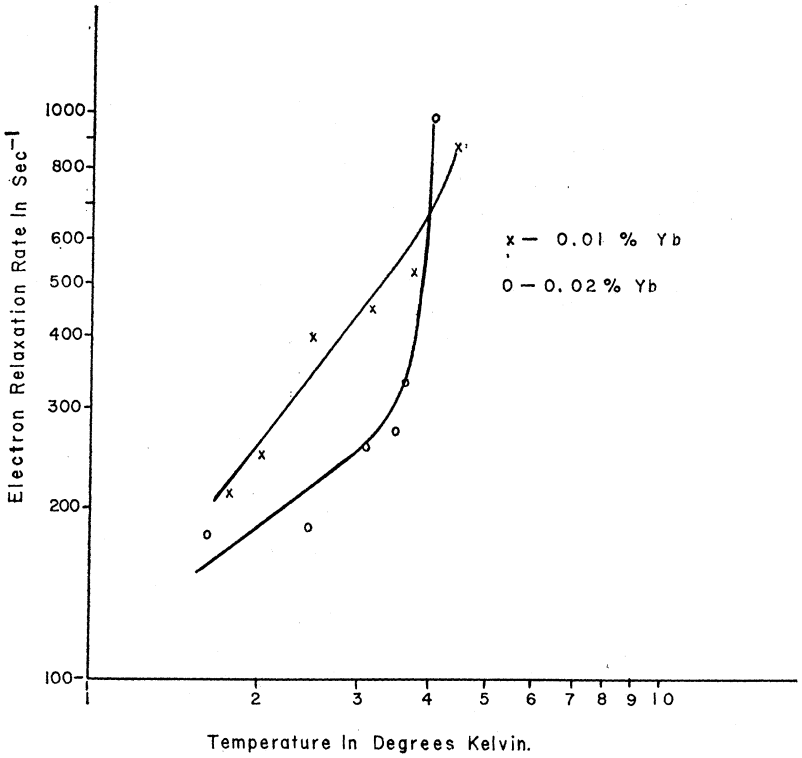

FIG. 7. Electron relaxation rate versus temperature, 0.01 and 0.02% Yb^{3+} in CaF_2.

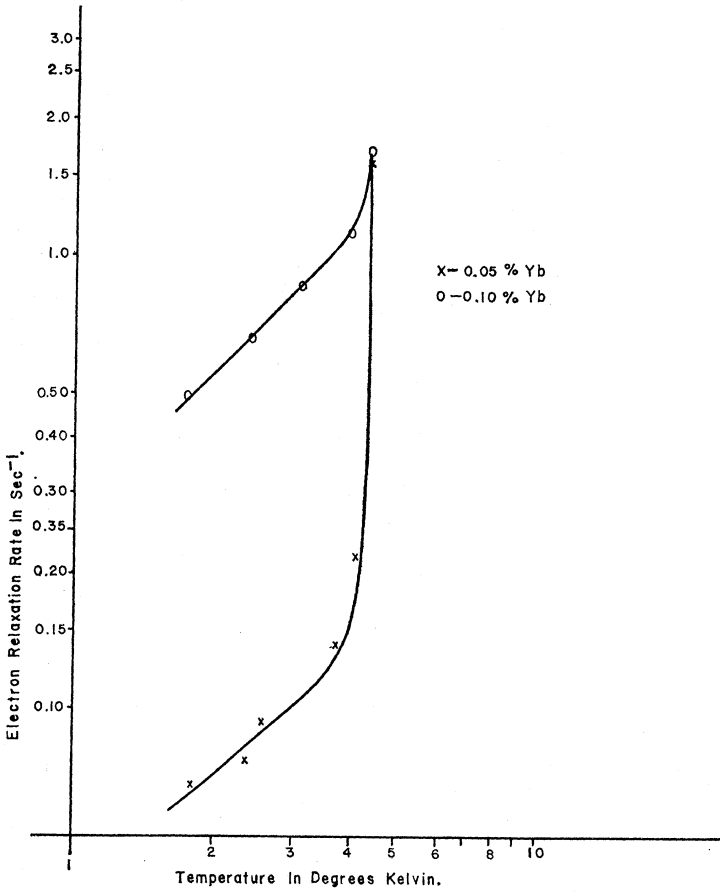

FIG. 8. Electron relaxation versus temperature, 0.05 and 0.10% Yb^{3+} in CaF_2.

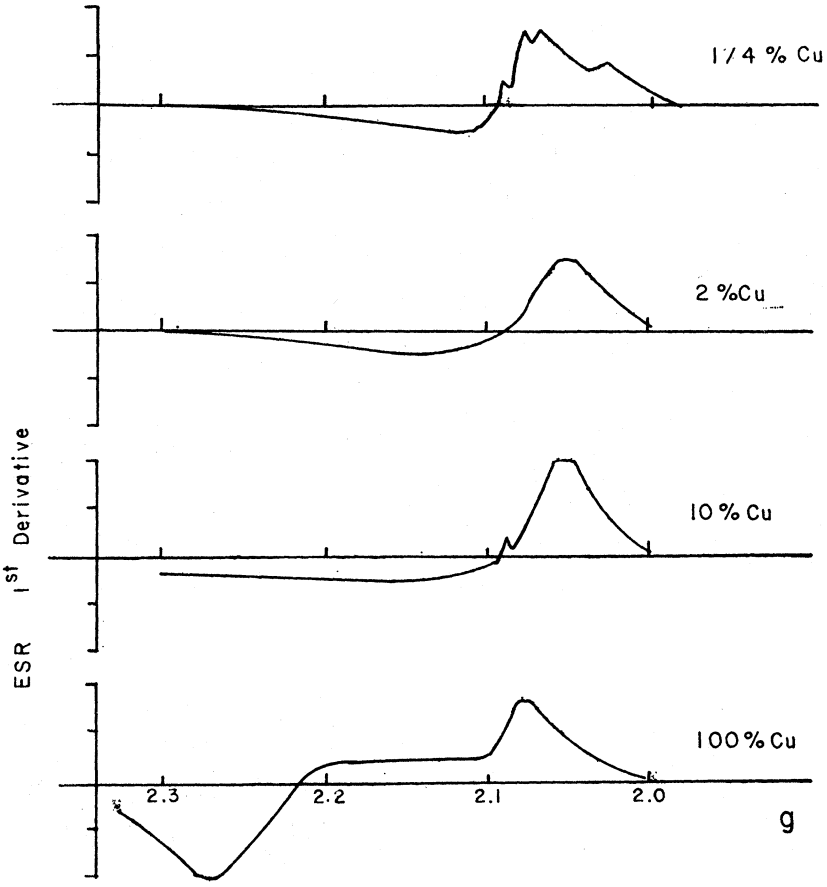

FIG. 9. ESR of Cu^{2+} in polycrystalline copper sulfate diluted by zinc sulfate.

and dynamic polarization measurements were performed with the magnetic field perpendicular to the g_{11} direction. ESR and enhancement curves for 0.05% Yb are shown in Fig. 5, where *Enh*= (enhanced amplitude)/(unenhanced amplitude)−1. The results show the solid-state effect, a maximum enhancement of 12, and a minimum of −10. Since the center of the enhancement curve falls at the center of the ESR line and the width of the ESR line is the same as the distance between the peaks of the enhancement curve, the observed enhancement belongs to Yb^{3+} in the trigonal site.

All samples show spin-diffusion-limited processes; and, therefore, the temperature dependence of spin-lattice relaxation may be obtained by multiplying the slope of the nuclear relaxation rate by 4. The nuclear

TABLE I. Relaxation results for Yb^{3+} in CaF_2 (T=3.0°K).

Concentration (%)	$1/T_N$ (sec^{-1}) (Expt)	$1/T_{1e}$ (sec^{-1}) [Eq. (31)]	Slope ($1/T_{1e}$ versus temp) (T<3.5°K)
0.01	0.14	260	0.7
0.02	0.25	470	1.4
0.05	0.085	0.10	0.9
0.10	0.80	0.85	1.0

δ=80 cm^{-1}, $1/T_{1e}$=0.15 sec^{-1} [Eq. (18)]

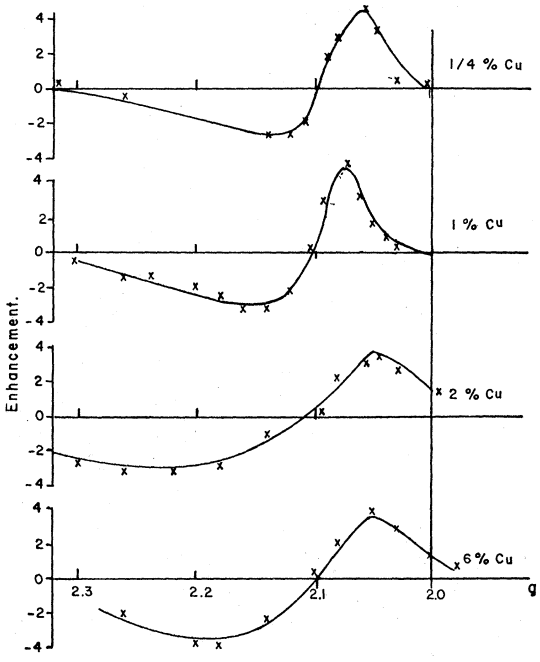

FIG. 10. Proton enhancement by Cu^{2+} in polycrystalline copper sulfate diluted by zinc sulfate.

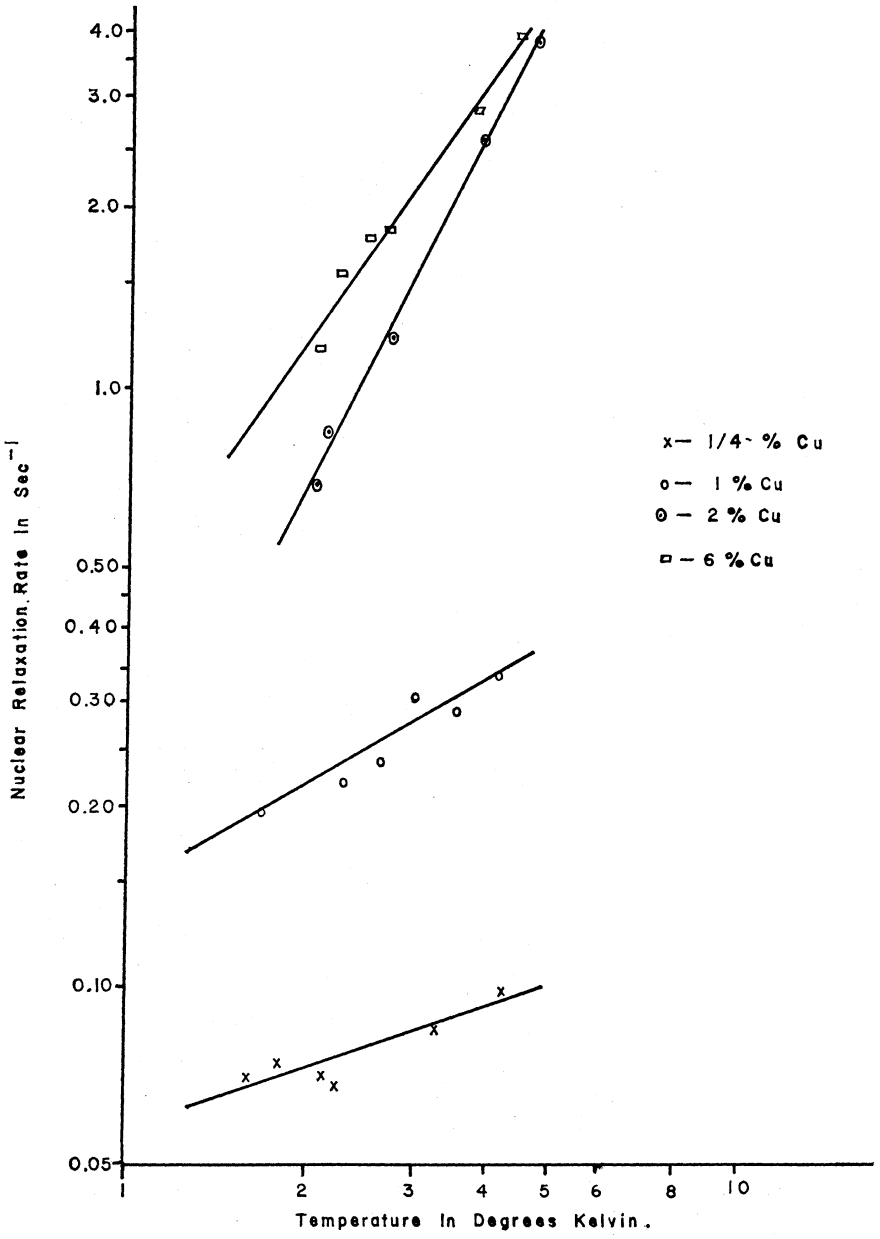

FIG. 11. Nuclear relaxation rate versus temperature; Cu^{2+} in copper sulfate diluted by zinc sulfate.

rate versus temperature is shown in Fig. 6 while the electron relaxation rate is shown in Figs. 7 and 8. The electron rate was calculated from Eq. (31) using the NMR linewidth (10 G) for T_{2n}, and an internuclear distance of 2.5 Å. As can be seen from these figures, the direct process predominates at low temperatures and it is superseded by a higher-order process in the range 3.6–4.2°K. This process will be shown to be of the Orbach type. Using $v=2.3\times10^5$ cm/sec, $\rho=2$ g/cc, and $T=3.0$°K, we find from Eq. (18), $T_{1e}=7$ sec which agrees, to order of magnitude, with Eq. (31) for concentrations of about 0.1%. An order of magnitude calculation of the Raman process will show that the higher-order process seen here must be the Orbach process. Since for the Raman process,[6]

$$(1/T_1)_R \simeq 256\pi^3(kT)^9/3h^7v^{10}\rho^2 \simeq 10^{-5} \text{ sec}^{-1}. \quad (33)$$

TABLE II. Relaxation results for Cu^{2+} in copper sulfate diluted by zinc sulfate ($T=3.0$°K).

Concentration (%)	$1/T_N$ (sec^{-1}) (Expt)	$1/T_{1e}$ (sec^{-1}) [Eq. (31)]	Slope ($1/T_{1e}$ versus temp)
¼	0.085	6.4	1.5
1	0.28	2.4	2.6
2	2.3	740	6.4
6	1.6	4.0	8.0

$\delta>100$ cm^{-1}, $1/T_{1e}=0.04$ sec^{-1} [Eq. (27)]

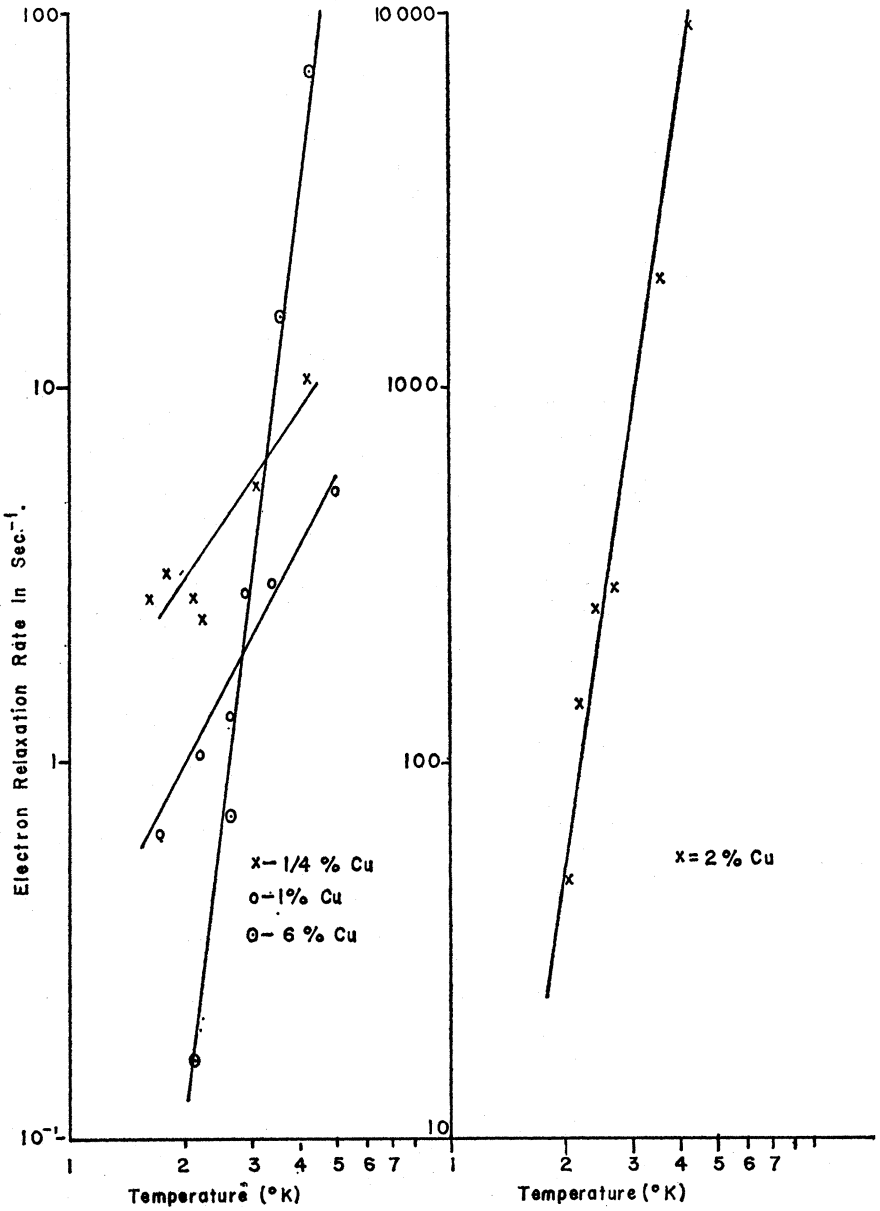

FIG. 12. Electron relaxation rate versus temperature; Cu^{2+} in copper sulfate diluted by zinc sulfate.

Five polycrystalline $CuSO_4 \cdot 5H_2O$ samples were prepared containing $\frac{1}{4}$, $\frac{1}{2}$, 1, 2, and 6% Cu^{2+}, respectively. Both ESR and dynamic polarization experiments were performed on these samples. (See Table II.) In addition, ESR measurements were made on polycrystalline samples of 10% Cu^{2+} (prepared as in Sec. III), and on crushed single crystals of 10 and 100% Cu^{2+}. Results for the two 10% samples were identical, showing that the structure at the paramagnetic site is the same. In addition, the main features of the ESR line are constant with concentration (Fig. 9), that is, a peak at $g=2.05$, zero at $g=2.1$, and a tail to $g\simeq 2.4$. Changes in the position of the low-field peak varied continuously with concentration, but concentration-dependent effects should be seen here because of an inequivalent Cu^{2+} site.[7] The enhancement curves are shown in Fig. 10; they show essentially the same features as the ESR line including the concentration-dependent effects. These two sets of curves indicate that the observed enhancement is due to Cu^{2+}, they also show the solid-state effect, and that the local site seen by the copper ion is the same at all concentrations investigated. Since the site is known to have the $5H_2O$ structure at 10 and 100% concentrations it can be seen that this structure is maintained locally when diluted by $ZnSO_4 \cdot 7H_2O$.

All samples showed spin-diffusion-limited processes and the nuclear relaxation rate as a function of temperature is shown in Fig. 11. The electron relaxation

rate is shown in Fig. 12. This was calculated from Eq. (31) for an NMR linewidth of 10 G and an internuclear distance of 1.6 Å. The direct process predominates at low concentrations and no evidence of the Orbach process is seen up to the experimental limit of 4.2°K. Estimates of λ have ranged from -370 to -700 cm^{-1}.[22–24] To calculate T_{1e}, the accepted value of λ for copper Tutton's salts, -695 cm^{-1}, is used. Using, then, $v=2.3\times10^5$ cm/sec, $\rho=2$ g/cc, $T=3.0$°K, $\Delta=12\,300$ cm^{-1},[22–24] and $g\beta H=\frac{1}{3}$ cm^{-1}, it is found that $T_{1e}=25$ sec [Eq. (27)].

VI. CONCLUSIONS

Enhancement of the NMR spectrum of protons in copper sulfate, and F^{19} nuclei due to Yb^{3+} in trigonal sites of CaF_2, may be observed. It is due to the solid-state effect and the decay rate of this enhancement may be correlated to the electron-spin-lattice relaxation rate. While observing the decay of the enhanced signal, it was found that the rf (NMR) power level was too small to appreciably affect the nuclear relaxation rate and therefore the nuclear relaxation measurements are valid.

In the case of Yb^{3+} the direct process predominates at temperatures below 3.6°K and the Orbach process predominates above 4.0°K. The change from direct to Orbach process is quite sharp owing to the large-temperature derivative of the Orbach process. The relaxation rate changed, for 0.05% Yb^{3+}, from 0.07 sec^{-1} at 1.8°K, to 0.10 sec^{-1} at 3.0°K, to 1.6 sec^{-1} at 4.2°K. From this data the first excited state energy was found to be $\simeq$80 cm^{-1} above the ground state. All samples indicated spin-diffusion processes.

Analysis of ESR data yields the $^2F_{7/2}$ wave functions and the splittings with an unknown scale factor. This factor may be determined from the above data.

In the case of Cu^{2+}, relaxation measurements were made for the direct process but the Orbach process was not detected, indicating that an estimate of the first excited state splitting must be greater than 100 cm^{-1}. All samples exhibited spin diffusion.

The Raman process was observed for Cu^{2+} at higher concentrations (Fig. 12). This is apparently due to a reduction of the triplet state splitting with increasing concentration. The relationship between the triplet state splitting and the strength of the Raman process is developed in Ref. 6.

It would be interesting to perform these experiments on single crystals of dilute copper sulphate and work is proceeding along this line.

ACKNOWLEDGMENTS

The authors wish to thank George Kemmerer and James Anderson of Temple University and Dr. Zdanek Sroubek of the Institute of Radio Engineering and Electronics, Czechoslovakia, for their kind assistance. They also wish to thank the Pitman-Dunn Research Laboratories, Frankford Arsenal, Philadelphia, Pa., for their generous support of this work.